(Supplementary Information)

Synthesis, characterization, self assembly and non-ohmic Schottky barier diode behaviors of two iron(III) based semiconductors with theoretical insight

Tanmoy Basak[a], Dhananjoy Das[b], Partha Pratim Ray[b], Snehasis Banerjee[c] and Shouvik Chattopadhyay

[a]*Department of Chemistry, Inorganic Section, Jadavpur University, Kolkata- 700032, India.*

[b]*Department of Physics, Jadavpur University, Kolkata- 700032, India.*

[c]*Govt. College of Engineering and Leather Technology, Salt Lake Sector-III, Block-LB, Kolkata 700106, India*

E-mail: [a]shouvik.chem@gmail.com, [b]parthapray@yahoo.com

Supramolecular interactions

The solid state structures of both complexes are stabilized through the non-covalent interactions, e.g. hydrogen bonding and C–H···π interactions. Complex **1**, forms a one dimensional array via intermolecular hydrogen bonding interactions where one hydrogen atom, H(2A), attached to an amine nitrogen atom, N(2), forms a hydrogen bond with the symmetry related methoxy oxygen atom, O(3)[a] {Symmetry transformation: [a]= 1/2-x,1/2+y,1/2-z} (Fig. **S1**). On the other hand, similar kind of interaction is observed for complex **2**, but here only dimer is formed by this interaction**.** The hydrogen atom, H(2A), attached to the amine nitrogen atom, N(2), is involved in a intermolecular hydrogen bonding interaction with the symmetry related phenoxo oxygen atom, O(1)[b] {Symmetry

transformation: [b]= 1-x,-y,1-z} (Fig. **S2**). For both complexes, the details of the hydrogen bonding interactions have been given in Table **4**.

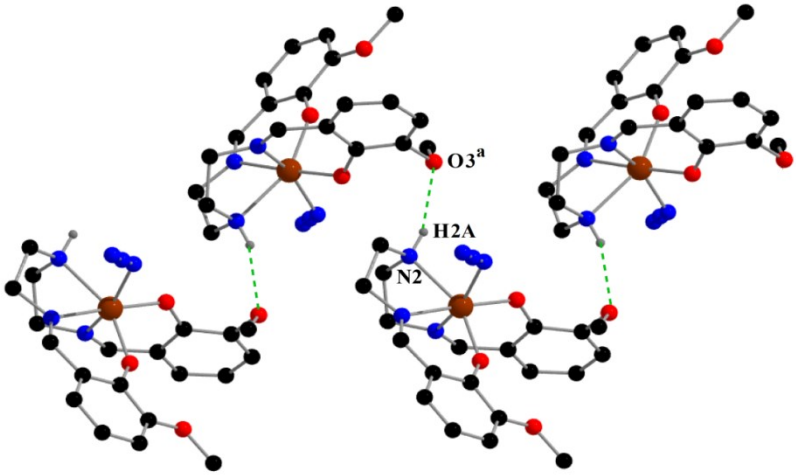

Fig. S1. One-dimensional array in complex **1**, generated through intermolecular hydrogen bonding interactions. Only the relevant hydrogen atoms are shown for clarity. [a]= 1/2-x,1/2+y,1/2-z.

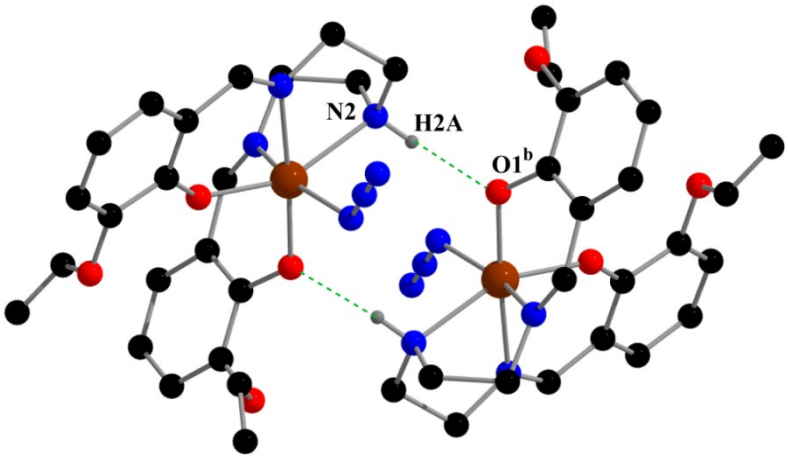

Fig. S2. Dimeric structure generated through intermolecular hydrogen bonding interactions in complex **2**. Only the relevant hydrogen atoms have been shown for clarity. [b]= 1−x,−y,1−z.

C–H···π interaction

For complex **1**, the hydrogen atom, H(11A), attached with the carbon atom, C(11), is involved in intermolecular C−H···π interaction with a phenyl ring C(13)−C(14)−C(15)−C(16)−C(17)−C(18). On the other hand, in complex **2**, the hydrogen atom,

H(8B), attached with the carbon atom, C(8), is involved in intermolecular C–H···π interaction with a phenyl ring C(13)–C(14)–C(15)–C(16)–C(17)–C(18). Another hydrogen atom, H(21B), attached with the carbon atom, C(21), is involved in intramolecular C–H···π interaction with a phenyl ring C(1)–C(2)–C(3)–C(4)–C(5)–C(6). The C–H···π interactions of both complexes are shown in Fig. **S3** and **S4**, respectively.

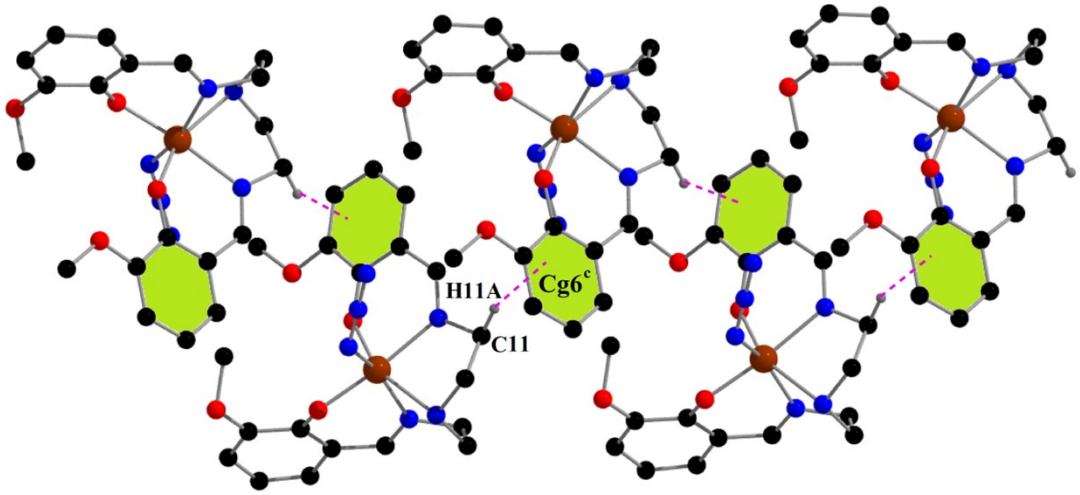

Fig. S3. One-dimensional array in complex **1**, generated through the Intermolecular C–H···π interaction. Only the relevant hydrogen atoms are shown for clarity.[c]= 3/2-x,1/2+y,1/2-z.

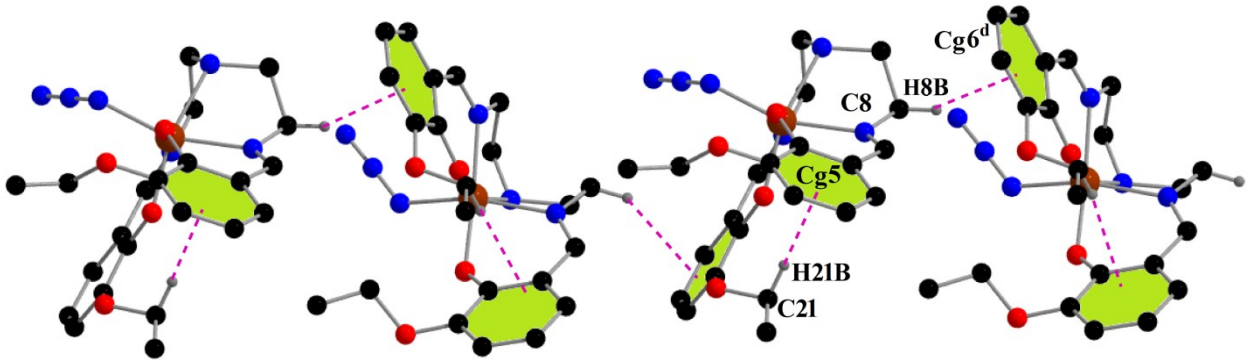

Fig. S4. One-dimensional array in complex **2**, generated through C–H···π interaction. Only the relevant hydrogen atoms are shown for clarity.[d]= x,1/2-y,1/2+z.

Table S1: Hydrogen bond distances (Å) and angles (º) in complexes **1** and **2**.

Complex	D-H···A	D-H	H···A	D···A	∠D-H···A
1	N(2)-H(2A)-O(3)[a]	0.90(3)	2.34(3)	3.201(3)	160(3)
2	N(2)-H(2A)-O(1)[b]	0.89(3)	2.02(3)	2.909(4)	174(2)

Symmetry transformations: [a]= 1/2-x,1/2+y,1/2-z; [b]= 1-x,-y,1-z.

Table S2: Geometric features (distances in Å and angles in °) of the C-H···π interactions obtained for complexes **1** and **2**.

Complex	C-H···Cg (Ring)	H···Cg (Å)	C-H···Cg (°)	C···Cg (Å)
1	C(11)-H(11A)···Cg(6)[c]	2.81	147	3.664(3)
2	C(21)-H(21B)···Cg(5)	2.96	158	3.879(6)
	C(8)-H(8B)···Cg(6)[d]	2.74	149	3.608(4)

Symmetry transformations: [c]= 3/2-x,1/2+y,1/2-z; [d]= x,1/2-y,1/2+z

Cg(5) = Centre of gravity of the ring [C(1)−C(2)−C(3)−C(4)−C(5)−C(6)]; Cg(6) = Centre of gravity of the ring [C(13) −C(14)−C(15)−C(16)−C(17)−C(18)].

Hirshfeld surfaces analysis

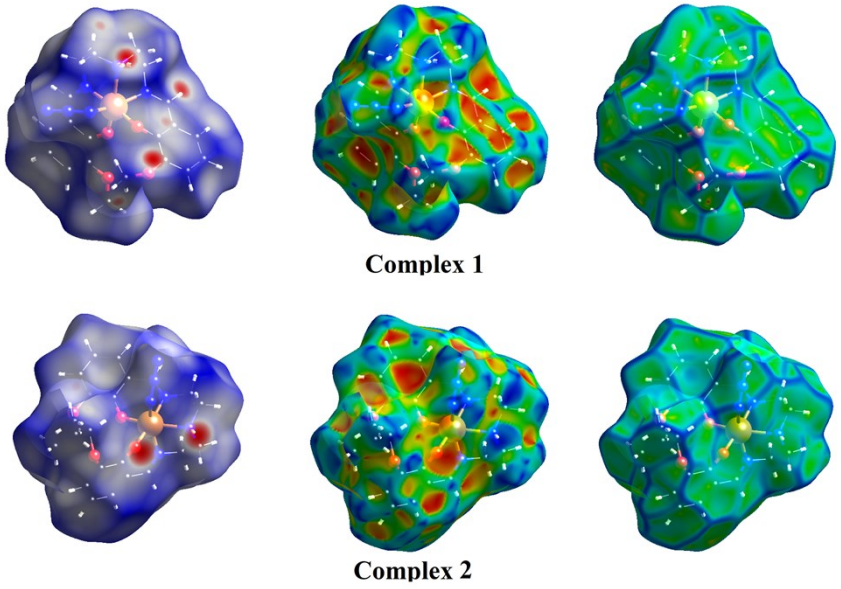

Fig. S5. Hirshfeld surfaces mapped with d_{norm} (left-side), shape index (middle) and curvedness (right-side).

IR specta

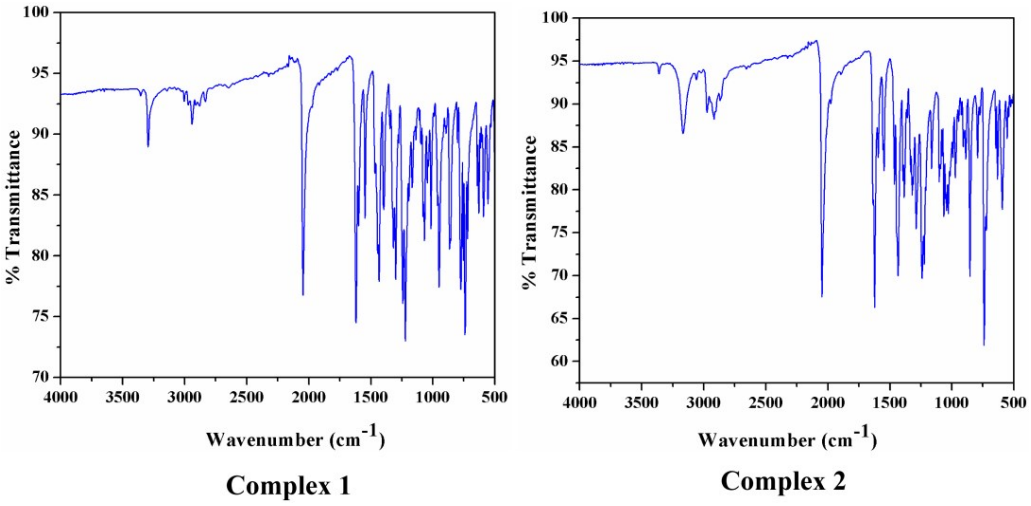

Fig.S6. IR plot of complexes **1** and **2**.

Device fabrication

To fabricate the Schottky diode, an ITO coated glass substrate was cleaned by using 2-propanol, acetone and distilled water sequentially and repeatedly. In parallel, we have

made a well-dispersed medium of the synthesized complex **1** and **2** in DMF (N, N-dimethylformamide) by ultra-sonicating for 2 hr. The as-prepared dispersed medium was coated onto the ITO coated glass substrate using the spin coating unit (SCU 2700) at the rate of 1000 rpm for 2 min. The as-prepared film was then dried in a vacuum oven. The thickness of the film was measured as 1μm. Finally, the aluminium electrode as metal contact was deposited using the Vacuum Coating Unit 12A4D of HINDHIVAC under pressure 10^{-6} Torr. The effective area of the Schottky contact deposited by shadow mask was measured as 7.065×10^{-6} m^{-2}.[1]

Analysis of diode parameters:

To estimate the energy band gap, we used the Tauc's equation, which is written as,[1]

$$(\alpha h\nu)^{m} = C\left(h\nu - E_{g}\right) \qquad \text{(S1)}$$

where α is the absorption coefficient, h is the Planck's constant, ν is the frequency of the light, C is an arbitrary constant, Eg is the optical band gap and m= 2 and ½ is corresponding to the allowed direct and indirect electronic transitions.

According to thermionic emission theory of Schottky diode, the current density of the fabricated diode can be expressed as,

$$J = J_0[e^{\frac{q_e V_0}{\eta k_B T}} - 1] \qquad \text{(S2)}$$

Where J_0 is the saturation current density, q_e is the electronic charge, V_0 is the voltage across the diode, η is the ideality factor, k_B is the Boltzmann constant and T is the absolute temperature. The saturation current density J_0 can be expressed as,[2]

$$J_0 = A^* T^2 e^{\frac{-q_e \phi_B}{k_B T}} \qquad \text{(S3)}$$

Where A^* is the effective Richardson constant and ϕ_B is the barrier height. Here, the effective diode area was measured as 7.065 × 10^{-6} m^2 and the effective Richardson constant was considered as 1.202 × 10^6 $Am^{-2}K^{-2}$.[3]

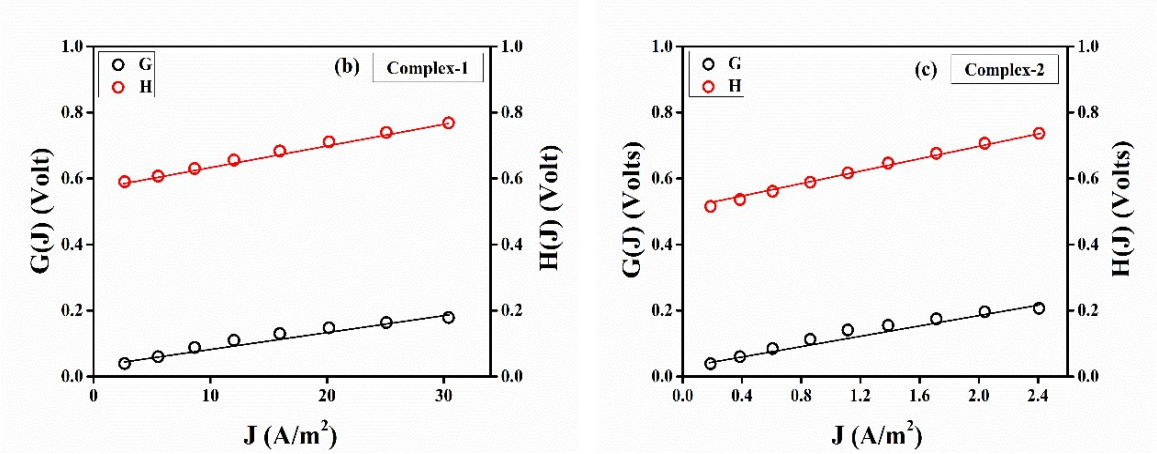

Fig. S7. G(J) and H(J) vs. J plot for **(b**) complex **1** and **(c)** complex **2**.

Using equation (S2) and (S3), two linear (Cheung's) equations (S4 and S5) were developed,[4] which helped us to find out the values of ideality factor (η), barrier height (ϕ_B) and series resistance (R_S) of the Al/complex/ITO configured metal-semiconductor diode.

$$G(J) = R_s A_{eff} J + \frac{\eta k_B T}{q_e} \qquad \text{(S4)}$$

$$H(J) = R_S A_{eff} J + \eta \phi_B \qquad \text{(S5)}$$

$$where,\ G(J) = \frac{dV}{d(\ln J)},$$

$$H(J) = V - \frac{\eta k_B T}{q_e} \ln\left(\frac{J}{A^* T^2}\right)$$

The ideality factor (η) which is a measure of the diode to be ideal for pure thermionic emission,[5] was determined from the intersection of the y-axis for the linear region of the equation (S4) (Fig. **S7**). The barrier height (ϕ_B) was estimated from the intersection of the equation (S5). The series resistance (R_S) was found both from equation (S4) and (S5) and the values of resistances are enlisted in Table 1 (main article) along with values of ideality factor and barrier height.

The dielectric constant of the complexes has been determined from the capacitance vs. frequency graph (Fig. **S8**) performed by two probe techniques. The value of capacitance at saturation (C_0) gives us the value of dielectric constant. The measured values of ε_r of both complex **1** and **2** are 0.41 and 5.88, respectively.[5]

$$\varepsilon_r = \frac{C_0 d}{\varepsilon_0 A_{eff}} \qquad \text{(S6)}$$

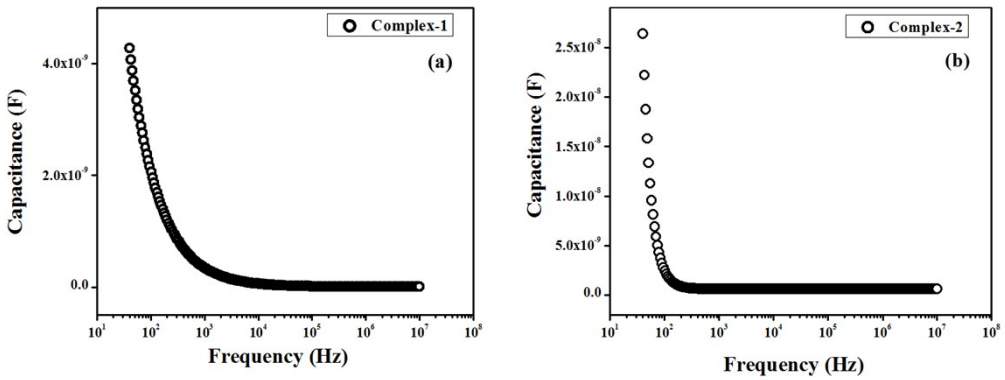

Fig: S8. Capacitance vs. frequency plot of (a) complex **1** and (b) complex **2**.

$$\varepsilon_r = \frac{C_0 d}{\varepsilon_0 A_{eff}} \qquad \text{(S7)}$$

References

1 J. Tauc, Amorphous and Liquid Semiconductors, Plenum Press, New York, 1974

2 R. Jana, A. Dey, M. Das, J. Datta, P. Das, P. P. Ray, Applied Surface Science, 2018, **452**, 155–164.

3 J. Datta, M. Das, S. Sil, S. Kumar, A. Dey, R. Jana, S. Bandyopadhyay, P. P. Ray, Materials Science in Semiconductor Processing, 2019, **91**, 133–145.

4 S. K. Cheung, N. W. Cheung, Appl. Phys. Lett., 1986, **49**, 85-87.

5 M. Sahina, H. Safaka, N. Tugluoglub and S. Karadeniz, Applied Surface Science 2005, **242**, 412–418.